1-1-1990

A Complete Model Characterization of Brushless DC Motors

N. Hemati

Ming-Chuan Leu
Missouri University of Science and Technology, mleu@mst.edu

Recommended Citation

N. Hemati and M. Leu, "A Complete Model Characterization of Brushless DC Motors," *Conference Record of the 1990 IEEE Industry Applications Society Annual Meeting, 1990*, Institute of Electrical and Electronics Engineers (IEEE), Jan 1990.
The definitive version is available at http://dx.doi.org/10.1109/IAS.1990.152182

A Complete Model Characterization of Brushless DC Motors

Neyram Hemati*
Assistant Professor
Department of Mechanical Engineering and Mechanics
Drexel University
Philadelphia, Pennsylvania 19104

Ming C. Leu*
Professor
Department of Mechanical and Industrial Engineering
New Jersey Institute of Technology
Newark, New Jersey 07102

Abstract This paper addresses the modeling problem associated with Brushless DC Motors (BLDCM) with non-uniform air gaps which operate in a range where magnetic saturation may exist. The mathematical model includes the effects of reluctance variations as well as magnetic saturation to guarantee proper modeling of the system. An experimental procedure is developed and implemented in a laboratory environment to identify the electromagnetic characteristics of a BLDCM in the presence of magnetic saturation. It is demonstrated that the modeling problem associated with this class of BLDCM can be formulated in terms of mathematically modeling a set of multi-dimensional surfaces corresponding to the electromagnetic torque function and the flux linkages associated with the motor phase windings. The accuracy of the mathematical model constructed by the developed method is checked against experimental measurements.

I. Introduction

In recent years, brushless motors have become a viable choice for motion control applications such as robotics, aerospace, numerically controlled machine tools, electric propulsion, and many more[1,3,15,16,21]. The increasing interest has been a consequnece of the advantages of brushless motors compared to the conventional DC motors. These advantages are mainly the result of the elimination of the physical contact between the mechanical brushes and commutators. Among the numerous types of brushless motors, the Brushless DC Motor (BLDCM) has emerged as the one with the highest potential in high performance applications[1,3,15,16]. In particular, BLDCM has been an attractive choice for direct drive applications[1,15], where large torques are required for high acceleration and deceleration rates. For such high performance applications, the mathematical model of BLDCM must include the effects of reluctance variations and, most importantly, the magnetic saturation whose existence is inevitable when large torques are generated.

In the past, due to the complexity involved, the tasks of modeling, analysis, and control of BLDCM have been based on a number of simplifying assumptions. Namely, the air gap has been assumed to be uniform and/or the magnetic structure has been assumed to be linear[1,3,9,11,14,15,17,18,20]. Persson and Buric[17] considered the mathematical modeling of BLDCM with arbitrary number of stator phase windings and permanent magnet pole pairs. Their work, however, was solely based on the assumption of having uniform air gaps and the absence of magnetic saturation. In [3], Demerdash et. al. presented digital simulation techniques to demonstrate the feasibility of using BLDCM for electric propulsion applications, where they cosidered BLDCMs with uniform air gaps and linear magnetic structures. The problem of optimal phase advancing to enhance the torque generation of BLDCM has been addressed by numerous authors, e.g. [11,14,20], whose results are based of the assumption that the reluctance variations are negligible. Krause et. al.[11] and Jahns [9] have used mathematical models which include the effect of reluctance variations to present some analytical results without addressing the saturation nonlinearity effects.

Another class of brushless motors which has attracted wide attention in the motion control industry is the Switched Reluctance Motor (SRM). Similar to BLDCM, SRM has also been the subject of numerous research projects and publications[2,7,8,13,19]. However, SRM constitutes a fundamentally different dynamical system than BLDCM. The difference lies in the fact that the phase windings of SRM are decoupled whereas in a BLDCM the coupling is significant. In other words, while it is common to neglect the effect of mutual inductances associated with the phase windings in a SRM, this is not a valid assumption in a BLDCM. The coupling among the phase windings introduces a significant problem which is resolved in section IV.

This paper presents a method of constructing accurate BLDCM models where both magnetic saturation and reluctance variation effects have been accounted for. It is demonstated that an accurate description of the characteristics of BLDCM may be obtained by modeling the torque function and the flux linkages associated with the stator phase windings as four-dimensional surfaces. However, for the mathematical model to be computationally feasible in real-time motion control applications, a method is presented which is used to reduce the complexity of the model without sacrificing its accuracy. For if the mathematical model is excessively complex, one will have to resort to incorporating look-up tables in real-time motion control applications[7]. To keep the complexity of the mathematical model within feasible limits, through physical reasoning it is demonstrated that the modeling problem may be reduced to that of identifying a set of two-dimensional surfaces. Based on this, a practical method for constructing accurate models of BLDCM is outlined and shown to be effectively implementable in a typical laboratory environment.

The paper is organized as follows. In section II the fundamental electromechanical characteristics of BLDCM are formulated in terms of a set of mathematical relationships. Section III sets forth some analytical results which are used to demonstrate the importance of including the effect of reluctance variations in the BLDCM model. Section IV deals with the problems associated with the modeling of the saturation nonlinearity for a BLDCM. Section V presents an experimental procedure which is used in identifying the mathematical model of BLDCM. The results corresponding to the set of experiments which have verified the validity of the methods described in the earlier sections are presented in section VI. Finally, some concluding remarks are made in section VII.

II. BLDCM without Magnetic Saturation

In the absence of magnetic saturation, the governing differential equations describing the dynamic behavior of BLDCM may be written as

$$\underline{V}(t) = \underline{R}\,\underline{I}(t) + \frac{d\underline{\Lambda}(\underline{I},\theta)}{dt} \qquad (1)$$

* Previously associated with the Sibley School of Mechanical and Aerospace Engineering, Cornell University, Ithaca, New York.

90/CH 2935-5/90/0000-0169$01.00©1990 IEEE

where θ is the position variable, $\underline{V}=[v_1,v_2,v_3]^T$ and $\underline{I}=[i_1,i_2,i_3]^T$ are the phase voltage input and current vectors, respectively. $\underline{R}$ is the resistance matrix, and the flux linkage vector is defined by

$$\Delta(\underline{I},\theta) = \underline{L}(\theta)\,\underline{I} + \Delta_m(\theta) \tag{2}$$

where the inductance matrix, $\underline{L}(\theta)$, is a 3-by-3, symmetric, positive definite matrix whose diagonal elements are the self inductances and the off-diagonal elements are the mutual inductances of the windings, and are defined by

$$L_{kk} = L_a - L_g \cos(2n\theta + \frac{2(k-1)\pi}{3}) \quad \text{for } k=1,2,3 \tag{3}$$

$$L_{12} = L_{21} = -\frac{L_a}{2} - L_g \cos(2n\theta - \frac{2\pi}{3}) \tag{4}$$

$$L_{13} = L_{31} = -\frac{L_a}{2} - L_g \cos(2n\theta - \frac{4\pi}{3}) \tag{5}$$

$$L_{23} = L_{32} = -\frac{L_a}{2} - L_g \cos(2n\theta) \tag{6}$$

L_a is the nominal (average) value of the winding inductance and L_g represents the amplitude of variation in the inductance due to the non-uniformity of the air gap. The elements of the permanent magnet flux linkage vector, $\Delta_m(\theta)$, i.e. λ_{mk}, k=1,2,3, represent the flux linkages associated with the permanent magnet and phase k. For sinusoidally distributed stator windings, λ_{mk} may be written as

$$\lambda_{mk} = K_e \sin(n\theta - \frac{2(k-1)\pi}{3}) \qquad k=1,2,3 \tag{7}$$

where K_e is the electromotive force constant, and n is the number of permanent magnet pole pairs. The expression for the torque generated by the motor as a function of phase currents and rotor displacement is

$$\begin{aligned} T(\underline{I},\theta) \;=\; & n L_g \{\, 2\,(\sin(2n\theta - \tfrac{2\pi}{3})\, i_1 i_2 \\ & + \sin(2n\theta + \tfrac{2\pi}{3})\, i_1 i_3 + \sin(2n\theta)\, i_2 i_3 \,) \\ & + \sum_{k=1}^{3} i_k^2 \cos(2n\theta + \frac{2(k-1)\pi}{3}) \;\} \\ & + nK_e \sum_{k=1}^{3} i_k \cos(n\theta - \frac{2(k-1)\pi}{3}) \end{aligned} \tag{8}$$

Equation (1) represents a system of differential equations with time varying (periodic) coefficients. It is known [4,10,22] that for sinusoidally distributed windings, a Floquet transformation, frequently referred to as the Park's transformation, may be used to transform the above equations to a system of differnetial equations with constant coefficients, represented in a coordinate frame attached to the rotor. This orthogonal transformation can be expressed in the matrix form as

$$\begin{bmatrix} \sigma_q & \sigma_d & \sigma_0 \end{bmatrix}^T = \sqrt{\frac{2}{3}} \begin{bmatrix} \cos(n\theta) & \cos(n\theta - \frac{2\pi}{3}) & \cos(n\theta + \frac{2\pi}{3}) \\ \sin(n\theta) & \sin(n\theta - \frac{2\pi}{3}) & \sin(n\theta + \frac{2\pi}{3}) \\ \frac{\sqrt{2}}{2} & \frac{\sqrt{2}}{2} & \frac{\sqrt{2}}{2} \end{bmatrix} \begin{bmatrix} \sigma_1 \\ \sigma_2 \\ \sigma_3 \end{bmatrix} \tag{9}$$

The subscripts 1,2,3 correspond to the stator windings, while the subscripts q, d, and 0 represent some fictitious windings attached to the rotor. The variables σ_1, σ_2, σ_3, σ_q, σ_d, and σ_0 may represent voltages, currents, or flux linkages. For convenience, we shall use a slightly different form of this transformation by replacing the last row in the transformation matrix by a row of $\frac{1}{2}$'s and replacing the scalar constant $\sqrt{\frac{2}{3}}$ by $\frac{2}{3}$. As a result, the transformed set of equations describing the behavior of BLDCM in the rotating frame become

$$v_q(t) = Ri_q(t) + n\lambda_d(t)\frac{d\theta(t)}{dt} + \frac{d\lambda_q(t)}{dt} \tag{10}$$

$$v_d(t) = Ri_d(t) + \frac{d\lambda_d(t)}{dt} - n\lambda_q(t)\frac{d\theta(t)}{dt} \tag{11}$$

where

$$\lambda_q(t) = L_q\, i_q(t) \tag{12}$$

$$\lambda_d(t) = L_d\, i_d(t) + K_e \tag{13}$$

and

$$L_q = (\frac{3}{2})(L_a - L_g) \tag{14}$$

$$L_d = (\frac{3}{2})(L_a + L_g) \tag{15}$$

The torque expression after application of the transformation becomes

$$T(i_q,i_d) = (\frac{3n}{2})\{\lambda_d(t)\, i_q(t) + \lambda_q(t)\, i_d(t)\} \tag{16}$$

In the following section the description of BLDCM in the rotating frame is used to show some analytical results, which compare the torque-speed characteristics of BLDCM with uniform and non-uniform air gaps.

III. Torque-Speed Characteristics of BLDCM

In the previous works related to the modeling of BLDCM, it has been common to neglect the reluctance variation terms [1,3,14,15,17,20]. In this section we will demonstrate that this may have adverse affects on the analytical results that one obtains. Figure 2 shows the torque-speed characteristics of the BLDCM whose specifications have been tabulated in Table I. The figure consists of the torque-speed (T-ω) plots of the BLDCM for the case when the reluctance variations have been accounted for and also when they have been neglected. As depicted in the figure, the reluctance variations affect the torque output in a favorable way. Accordingly, some researchers, e.g.[9], have used this desirable factor to design permanent magnet motors with better torque producing capabilities by introducing significant saliency in the motor. Here, we will demonstrate the adverse affect of neglecting the reluctance variations on the motor characteristics by considering the optimal phase advancing scheme[11,14,20].

For the constant speed operation of BLDCM, the voltage inputs accross the stator phase windings may be written as

$$v_k = V_{max} \cos(n\theta - \frac{2(k-1)\pi}{3} - \phi) \qquad k=1,2,3 \tag{17}$$

where ϕ is a phase shift which may be varied to alter the torque-speed characterisitcs of the motor. When the reluctance variations

are neglected, the torque generated as a function of the phase shift ϕ may be written as

$$T(\phi) = \{\frac{3nK_eR}{2[R^2+(nL_q\omega)^2]}\} \{V_{max}[\cos(\phi) - (\frac{nL_q\omega}{R}) \sin(\phi)] - nK_e\omega\} \quad (18)$$

The torque function, equation (18), has a maximum at

$$\phi = - tan^{-1} (\frac{nL_s\omega}{R}) \quad \text{where } \frac{-\pi}{2} < \phi < 0 \quad (19)$$

which is referred to as the "optimal phase advance"[14,20]. Figure 3 shows the effect of the optimal phase advance on the torque-speed characteristics of the BLDCM assuming that the air gap is uniform. However, if this "optimal" phase advance is incorporated in altering the characteristics of the actual motor, i.e. the non-uniform air-gap motor, then the enhancement in the T-ω plots will only exist at high operating speeds; see figure 4. As depicted in this figure, the incorporation of the "optimal" phase advance computed based on a uniform air-gap model actually degrades the T-ω characteristics at lower operating speeds. This degradation would be even more pronounced if the BLDCM were to have more significant variations in its air gap reluctance; see figure 5. These suggest that in order to enhance the T-ω characteristics of the non-uniform air-gap BLDCM the optimal phase advance must be computed based on the model which includes the effect of reluctance variations.

When the reluctance variations have been taken into account, and for a constant rotor speed, the torque equation as a function of ϕ may be written as

$$T(\phi) = (\frac{3n}{2})[K_e + (L_d - L_q)\frac{n\omega L_q i_q + V_{max} \sin(\phi)}{R}] i_q \quad (20)$$

where

$$i_q = \frac{V_{max}[\cos(\phi) - \frac{n\omega L_d}{R} \sin(\phi)] - nK_e\omega}{R(1 + \frac{n^2\omega^2 L_d L_q}{R^2})} \quad (21)$$

To determine the value of ϕ which would maximize $T(\phi)$, it is necessary to use numerical techniques. Figure 6 shows the torque-speed characteristics of the BLDCM for both the normal operation, i.e. ϕ=0, and when the optimal phase advance, computed by maximizing $T(\phi)$ in equation (20), has been incorporated.

IV. BLDCM with Magnetic Saturation

In this section we will consider the presence of magnetic saturation. A procedure will be outlined and then implemented for construction of accurate BLDCM mathematical models when magnetic saturation and reluctance variations are present. In section II the flux linkages were in terms of constant inductance parameters, see equations (2)-(6). However, when magnetic saturation is present, the flux linkages are no longer linear functions of the phase currents, and one can only state that

$$\lambda_k = \lambda_k (i_1, i_2, i_3, \theta) \qquad k = 1, 2, 3 \quad (22)$$

In other words, the flux linkages define a set of 4-dimensional surfaces in a 5-dimensional space. It is possible to experimentally obtain these flux linkage surfaces. Recalling equation (1) and for a fixed value of $\theta = \theta^*$, one can write

$$\lambda_k (i_1, i_2, i_3, \theta^*) = \int_0^t [v_k(\tau) - Ri_k(\tau)] \, d\tau \quad (23)$$

This may be used in constructing the flux linkage surfaces as follows. By appropriately varying phase voltages, v_k, or currents, i_k, and sampling their values, the integral in equation (23) can be computed. The corresponding values of the integral will then define a set of discrete data points which lie on the flux linkage surfaces. Using numerical techniques, one can then compute approximate mathematical representations for these surfaces. Once a set of mathematical representations for the flux linkages have been obtained, one can then derive the torque expression by first constructing the coenergy function

$$W_c(i_1, i_2, i_3, \theta) = \int_0^{i_1} \lambda_1(\theta, \xi, 0, 0) \, d\xi + \int_0^{i_2} \lambda_2(\theta, i_1, \eta, 0) \, d\eta + \int_0^{i_3} \lambda_3(\theta, i_1, i_2, \zeta) \, d\zeta \quad (24)$$

and then

$$T(i_1, i_2, i_3, \theta) = \frac{\partial W_c(i_1, i_2, i_3, \theta)}{\partial \theta} \quad (25)$$

where in equation (24) ξ, η, and ζ are dummy variables of integration.

Our main purpose for constructing an accurate mathematical model for BLDCM has been to be able to incorporate it in control applications. However, the modeling procedure stated above will result in complex mathematical relationships, which are computationally unattractive for real-time control purposes. Furthermore, as illustrated in equation (25) the torque expression explicitly depends on rotor displacement which leads to the need for constructing explicit commutation strategies. This could make the real-time control of BLDCM with magnetic saturation infeasible. In the following subsection a different approach is presented which eliminates the need for such a complex model formulation.

IV.a. BLDCM Model in Rotating Frame

In the absence of magnetic saturation, Park's transformation was used in section II to obtain a simplified formulation for BLDCM in a rotating frame attached to the rotor. This eliminated the dependence of the inductance parameters and the torque expression on the rotor displacement. However, when magnetic saturation is present, Park's transformation does not apply, if the flux linkages are expressed by nonlinear functions. To render this transformation valid, we formulate the behavior of the BLDCM with magnetic saturation by a piecewise linear model. In other words, the flux linkages are modeled by piecewise linear functions of the phase currents. This in turn allows us to apply the Park's transformation to obtain a simplified description of BLDCM with magnetic saturation. The parameters defining the flux linkages, i.e. inductances and electromotive force constant, now become piecewise constant functions of the phase currents. The BLDCM with magnetic saturation is represented in the rotating frame by a set of equations similar to equations (10)-(15) except that now the inductance parameters L_a and L_g and the electromotive force constant K_e are piecewise constant functions of the phase currents.

This in turn defines a piecewise linear model for the flux linkages, λ_q and λ_d.

Consequently, the characteristics of the saturated BLDCM are described by three piecewise constant functions of current: $L_a(i)$, $L_g(i)$, and $K_e(i)$. Since the flux linkages corresponding to the individual phase windings are all functions of these three parameters, the experimental identification process may be performed for each phase winding independent of the rest. Considering one phase winding at a time, we have

$$\lambda_k (i_k, i_j = 0, i_m = 0, \theta) = \lambda_k (i_k, \theta) \qquad j, k, m = 1,2,3, \ j \neq k \neq m \qquad (26)$$

The flux linkage, λ_k, now represents a 2-dimensional surface rather than a 4-dimensional surface. As was done in equation (23), we can now write

$$\lambda_k (i_k, \theta) = \int_0^t [v_k(\tau) - R i_k(\tau)] \, d\tau \qquad k = 1,2,3 \qquad (27)$$

The surfaces representing the flux linkages may then be constructed by sampling the voltage, v_k, and the current, i_k, and computing the integral in equation (27). Once a sufficient number of data points on the flux linkage surfaces have been collected, we can obtain a mathematical representation for each of these surfaces by using numerical optimization techniques. This will be discussed in section VI.

Usually, in a BLDCM the resistance R is much larger in value than the inductances L_a and L_g. Consequently, for the inductance voltage drop, $L\frac{di_k}{dt}$, to be in the same order of magnitude as the resistance voltage drop, Ri_k, the time rate of change of current must be very large. In performing experiments, this large current rate is needed if the voltage information is to be used to determine an accurate description of the flux linkages. However, this requires a power supply capable of providing currents at high frequencies and in turn results in the need for expensive instrumentation. To remedy this problem, we use an alternative approach for performing experiments and data collection as presented below.

V. Experimental Determination of BLDCM Model

The experimental procedure outlined in section IV can be implemented satisfactorily only if appropriate power supplies and instrumentation are available. To remedy these limitations, we have based our experimental method on the following alternative approach. The method incorporates torque and current measurements, for the rotor locked at various rotor displacements, to construct the coenergy function associated with the BLDCM. The coenergy function is expressed as

$$W_c(i,\theta) = \Phi(i,\theta) + \Psi(i) \qquad (28)$$

where

$$\Phi(i,\theta) = \int T(i,\theta) \, d\theta \qquad (29)$$

and $\Psi(i)$ is related to the part of winding inductance which is independent of the rotor position, i.e. L_a.

By conducting torque measurements at a sufficient number of points in the *phase current-rotor displacement* plane, a 2-dimensional surface representing the torque surface is constructed. By computing the integral in equation (29), $\Phi(i, \theta)$ can be obtained. Separate measurements are then conducted to identify $\Psi(i)$.

The torque produced in BLDCM is due to the interaction of the permanent magnet with the magnetic field created by the current flow in the stator windings and also the reluctance effect. If only one phase (line-to-line) is conducting, the torque equation (8) is reduced to

$$T(i,\theta) = nL_G \sin(2n\theta - 2\phi) \, i^2 + nK_E \cos(n\theta - \phi) \, i \qquad (30)$$

where $L_G = 3 L_g$ and $K_E = \sqrt{3}K_e$. When the saturation effect is taken into account, the parameters K_E and L_G cannot be assumed constant, and as a result equation (30) does not accurately describe the behavior of the system. However, since a piecewise linear model is considered to characterize the saturation effect, it is assumed that the sinusoidal distribution of the phase windings does not change with the current variations. In other words, we will assume that the functional dependence of the torque on the rotor displacement is preserved and only the amplitudes of the two sinusoids in equation (30) vary as functions of current. The torque expression for the case when magnetic saturation is present may then be written as

$$T(i,\theta) = \alpha(i) \cos(n\theta - \phi) \, i + \beta(i) \sin(2n\theta - 2\phi) \, i^2 \qquad (31)$$

where

$$\alpha(i) = n K_E(i) \qquad (32)$$

$$\beta(i) = n L_G(i) \qquad (33)$$

V.a. Torque Measurement: Identification of $\Phi(i,\theta)$

An experimental procedure has been designed to identify the parameters describing the characteristics associated with each line-to-line phase winding. In the experiments, one leg of the Y-connected stator phase windings is removed and the two remaining legs carry the same amount of current at all times. The rotor is locked at a fixed position when a prescribed current is supplied to the windings; see figure 7. As the current rises and falls, so does the torque generated by the motor. During these variations, torque and current measurements are taken at discrete points of time. The same procedure is repeated for several rotor positions. Finally, a set of measured torques at discrete points in the $(i\text{-}\theta)$ plane are collected. Since the identification process is based on torque measurements, the frequency of the current input is kept low.

Figures 8 and 9 show the sample data collected at different rotor positions and different current values. The curves in the figures define various cross sections of the torque surface. Keeping θ constant corresponds to the curve generated by intersecting a plane parallel to the (T-i) plane with the torque surface, while keeping i constant corresponds to the curve generated by intersecting a plane parallel to the $(T\text{-}\theta)$ plane with the torque surface. By experimentally determining sets of such curves, the torque surface is constructed. Notice that the curves in figures 8 and 9 show the presence and degree of hysteresis in the magnetic structure. The hysteresis is due to the fact that the current supplied to the windings follows a cycle of triangular signal with a peak value.

V.b. Inductance Measurement: Identification of $\Psi(i)$

The term $\Psi(i)$ in the coenergy function, equation (28), depends only on current and cannot be detemined by torque measurements alone. In the case of a linear magnetic structure, this term appears in the flux linkage formulation as the inductance term which is independent of rotor displacement, i.e.

$$\Psi(i) = \frac{1}{2} L_A \, i^2 \qquad (34)$$

The inductance parameters L_A and L_G may be written in the following way[4,9]:

$$L_A = K_A \mu \tag{35}$$

$$L_G = K_G \mu \tag{36}$$

where K_A and K_G are constant parameters which are solely functions of the geometry of the rotor and the windings, and μ is the permeability factor. Since a piecewise linear model has been considered for the case of magnetic saturation, one can write

$$\frac{L_A(i)}{L_G(i)} = \text{constant} \tag{37}$$

Since $L_G(i)$ has already been determined as a result of identifying $\Phi(i, \theta)$, it is sufficient to determine the value of L_A in the linear range of operation, and then use equation (37) to evaluate $L_A(i)$. To measure L_A in the linear range, an inductance analyzer is used to directly measure the inductance of the windings.

VI. Experimental Results

The torque data at discrete values of rotor displacements and phase currents are fitted to an analytical torque surface of the form given in equation (31), where $\alpha(i)$ and $\beta(i)$ are assumed piecewise polynomials of current i. For the BLDCM studied here, three polynomials are used to represent $\alpha(i)$ and $\beta(i)$ for three separate intervals of current. The parameters defining the polynomials are computed by fitting the best torque surface defined by (31) to the torque data in the least square error sense. The piecewise polynomial functions are required to be continuous and to have continuous first derivatives since

$$\lambda(i, \theta) = \frac{\partial[\int T(i,\theta)\, d\theta + \Psi(i)]}{\partial i} \tag{38}$$

which implies that the torque expression must be at least C^1 in i.

The torque surface fitting problem may be formulated as a least square problem as follows

$$\min \| T(i,\theta) - T_d(i,\theta) \|_F \tag{39}$$

where T_d is the matrix containing the torque data and F denotes the Frobenius matrix norm. The expression defining the torque surface, equation (31), may be written in the following form

$$T(i,\theta) = T_1(i,\theta) + T_2(i,\theta) \tag{40}$$

where

$$T_1(i,\theta) = \alpha(i) \cos(n\theta)\, i = (\alpha_0 + \alpha_1 i + \alpha_2 i^2 + \cdots) \cos(n\theta)\, i \tag{41}$$

$$T_2(i,\theta) = \beta(i) \sin(2n\theta)\, i^2 = (\beta_0 + \beta_1 i + \beta_2 i^2 + \cdots) \sin(2n\theta)\, i^2 \tag{42}$$

Figures 10 through 13 show the resultant approximating functions fitted to the experimental data at various values of θ and i. To see the overall behavior of the torque generated by one phase winding as a function of rotor position and phase current, figure 14 depicts the torque surface generated by the mathematical model. To further examine the accuracy of the mathematical model, a set of independent experimental data are used. Figure 15 depicts the predicted values of the line-to-line phase winding inductance as a function of rotor displacement compared with the experimental data. Figure 16 shows the torque-current data of the BLDCM at a constant rotor speed. The agreement between the predicted values and the experimental data are quite good, specially considering that this set of experimental data is taken from a different motor unit than the one used for the construction of the mathematical model.

VII. Conclusions

An analytical and experimental study of brushless DC motors has been presented. A method for constructing a BLDCM model has been presented which accounts for magnetic saturation and reluctance variation effects. Based on a piecewise linear magnetic structure, an experimental procedure has been outlined and implemented to identify the parameters describing the characteristics of a BLDCM. Using the experimental data obtained from torque and phase current measurements, a mathematical model of the two-dimensional torque surface was obtained by solving the corresponding least squares problem. The accuracy of the resulting mathematical model was successfully checked against independent experimental measurements.

VIII. Acknowledgements

The authors thank professor J. S. Thorp of Cornell University for many valuable discussions and comments. This project was funded in part by Moog Inc., East Aurora, New York, and by the NSF grant MSM8451074.

IX. References

[1] Asada, H., and Youcef-Toumi, K., "Direct Drive Robots: Theory and Practice", MIT Press, 1987.

[2] Chai, H. D., "Permeance Model and Reluctance Force Between Toothed Structures", In Theory and Applications of Step Motors, West Publishing Co., 1974.

[3] Demerdash, N.A., Nehl, T.W., and Maslowski, E., "Dynamic Modeling of Brushless DC Motors in Electric Propulsion and Electromechanical Actuation by Digital Techniques", IEEE/IAS Conference Record, Cincinnati, pp. 570-579, 1980.

[4] Fitzgerald, A.E., Kingsley, C., and Umans, S.D., "Electric Machinery", Fourth Edition, McGraw-Hill, 1983.

[5] Hemati, N., "Modeling, Analysis, and Tracking Control of Brushless DC Motors for Robotic Applications", Ph.D. Thesis, Sibley School of Mechanical and Aerospace Engineering, Cornell University, August 1988.

[6] Hemati, N., and Leu, M., "Accurate Modeling of Brushless DC Motors for High-Performance Applications", Proc. 18th annual symp. Incremental Motion Control Systems and Devices, June 1989.

[7] Ilic-Spong, M., Marino, R., Peresada, S. M., and Taylor, D. G., "Feedback Linearizing Control of Switched Reluctance Motors", IEEE Trans. on Automatic Control, vol. AC-32, No. 5, pp. 371-379, May 1987.

[8] Ilic-Spong, M., Miller, T.J.E., MacMinn, S.R., and Thorp, J.S., "Instantaneous Torque Control of Electric Motor Devices", IEEE Trans. on Power Electronics, vol. PE-2, No. 1, pp.55-61, Jan. 1987.

[9] Jahns, T.M., "Torque Production in Permanent-Magnet Synchronous Motor Drives with Rectangular Current Excitation", IEEE Trans. on Ind. Appl., IA-20, No.4, pp. 803-813, July/August 1984.

[10] Krause, P.C., "Analysis of Electric Machinery", McGraw-Hill, 1986.

[11] Krause, P.C., Nucera, R.R., Krefta, R.J., Wacynczuk, O.,"Analysis of A Permanent Magnet Synchronous Machine Supplied from a 180° Inverter with Phase Control", IEEE

Trans. on Energy Conversion, vol. EC-2, No.3, pp. 423-431, Sept. 1987.

[12] Lawson, C.L., and Hanson, R.J., Solving Least Squares Problems, Prentice-Hall, 1974.

[13] Manzer, D.G., and Verghese, M., "Robot Motor Modelling Revisited: A Complete 3-D Characterization", IBM Technical Report, July 1987.

[14] Meshkat, S., "A New Microprocessor Based Brushless Servo Amplifier for Optimum Current Vector Control", Proc. 13th IMCSD annual symp., pp. 19-24, 1984.

[15] Muir, P., Neuman, C.,"Pulsewidth Modulation Control of Brushless DC Motors for Robotic Applications", IEEE Trans. on Industrial Electronics, vol.IE-32, No.3, pp.222-229, Aug. 1985.

[16] Murugesan, S., "An Overview of Electric Motors for Space Applications", IEEE Trans. on Ind. Elec. and Control Inst., Vol. IECI-28, No. 4, Nov. 1981.

[17] Persson, E.K., and Buric, M., "Mathematical Modelling and Simulation of High Performance Brushless DC Motors", IMCSD 5th annual symp., pp. W1-W8, 1976.

[18] Pfaff, G., Weschta, A., and Wick, A., "Design and Experimental Results of A Brushless AC Servo-Drive", IEEE Trans. on Ind. Appl., vol. IA-20, No. 4, pp.814-821, July/August 1984.

[19] Ray, W. F., Lawrenson, P. J., Davis, R. M., Stephenson, J. M., Fulton, N. N., and Blake, R. J., "High Performance Switched Reluctance Brushless Drives", IEEE/IAS, pp. 1769-1776, 1985.

[20] Tal, J.,"Optimal Commutation of Brushless Motors", IMCSD 11th annual meeting, pp. 49-53, 1982.

[21] Vidyasagar, M., "System Theory and Robotics", IEEE Control Systems Magazine, pp. 16-17, April 1987.

[22] Youla, D.C., and Bongiorno, J.J., Jr., "A Floquet Theory of the General Rotating Machine", IEEE Trans. on Circuits and Systems, vol. CAS-27, No. 1, pp. 15-19, Jan. 1980.

Parameter	n	R	Ke	La	Lg
Unit	—	Ohm, Ω	v/rad/s	milli-Henries	milli-Henries
Numerical value	4	0.9	0.02502	0.95	0.2

Table I: Numerical values for the parameters of an unsaturated BLDCM.

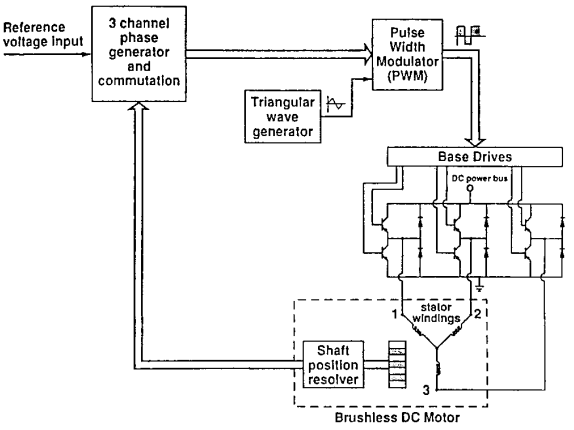

Figure 1: A typical Brushless DC Motor and its commutation.

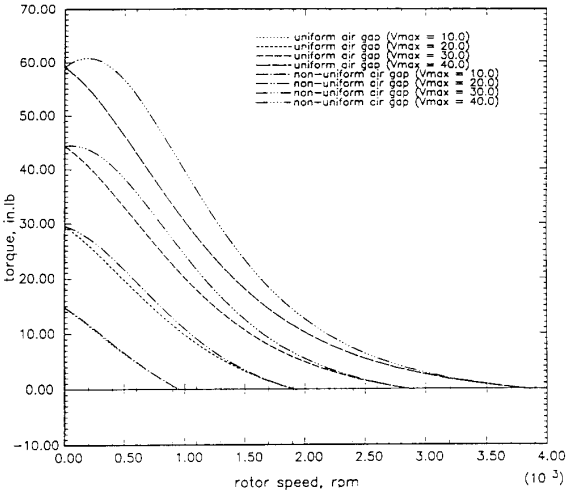

Figure 2: Torque-speed characteristics of the uniform and non-uniform air-gap BLDCM models.

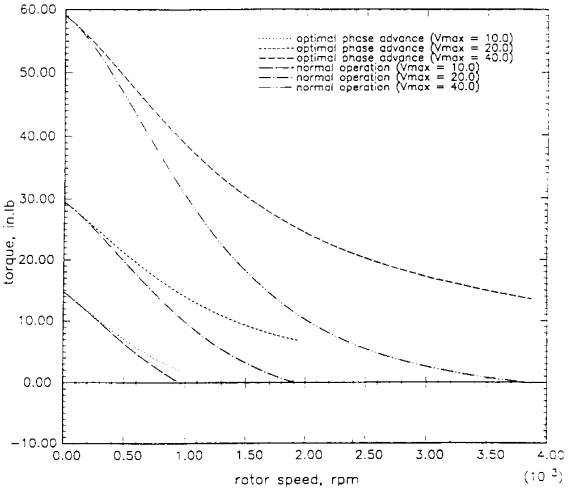

Figure 3: Torque-speed characteristics of the uniform air-gap BLDCM with and without optimal phase shift in the voltages accross the phase windings.

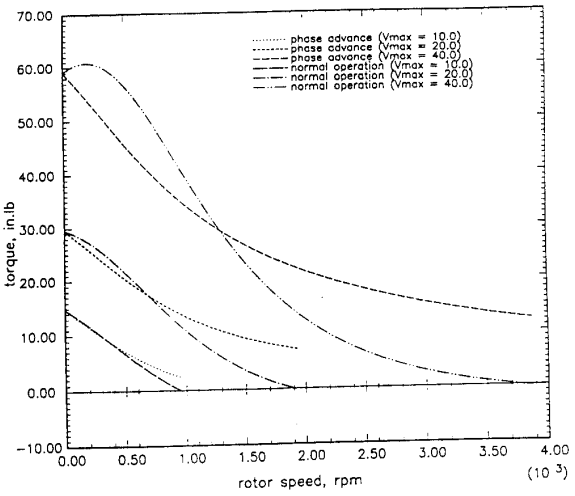

Figure 4: Torque-speed characteristics of the non-uniform air-gap BLDCM for the normal operation and for the operation when the phase shift is computed based on the uniform air-gap model.

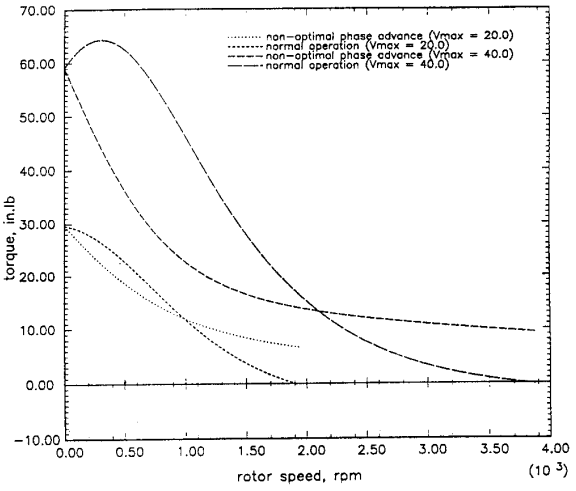

Figure 5: Torque-speed characteristics of the non-uniform air-gap BLDCM with twice saliency, for the normal operation and when the phase shift is computed from the uniform air-gap model.

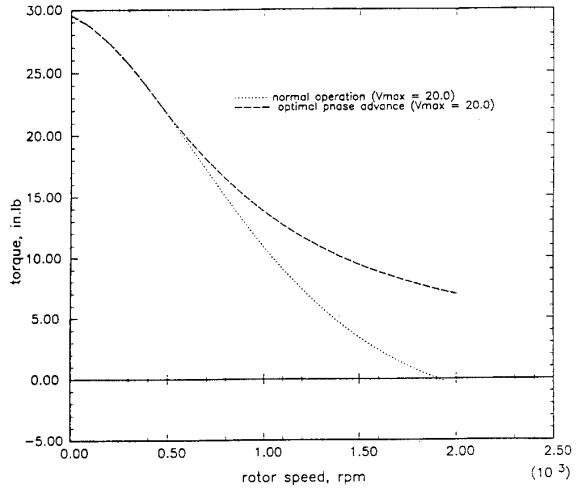

Figure 6: Torque-speed characteristics of the non-uniform air-gap BLDCM with and without optimal phase shift in the voltage inputs.

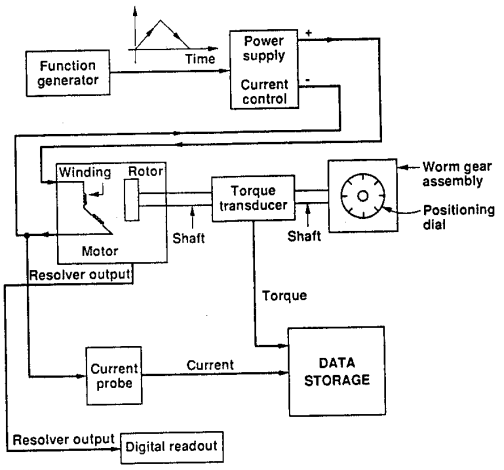

Figure 7: Experimental set-up for torque and current measurements.

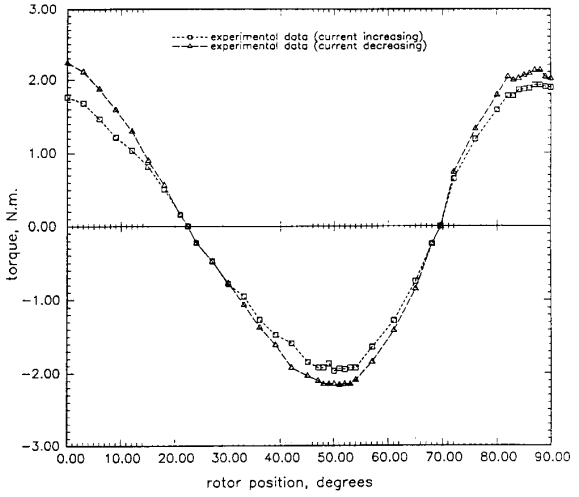

Figure 8: Experimental torque measurements, i=7.5 amperes.

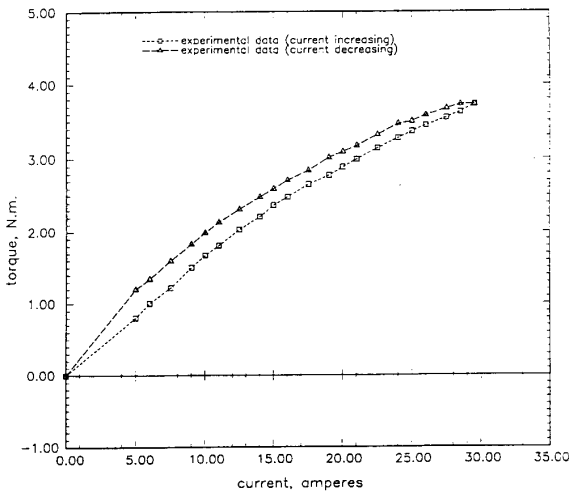

Figure 9: Experimental torque measurements, θ=9.0 degrees.

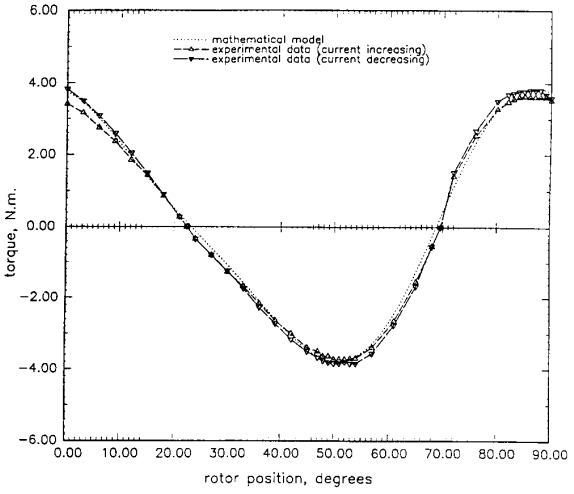

Figure 10: Experimental and modelled torque values, i=15 amps.

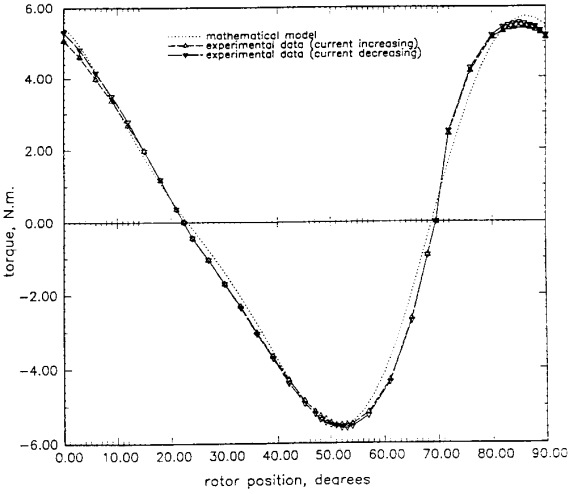

Figure 11: Experimental and modelled torque values, i=25 Amps.

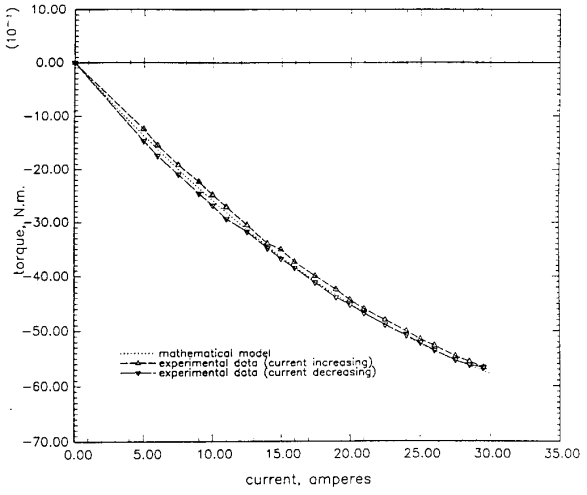

Figure 12: Experimental and modelled torque values, θ=47.0 degrees.

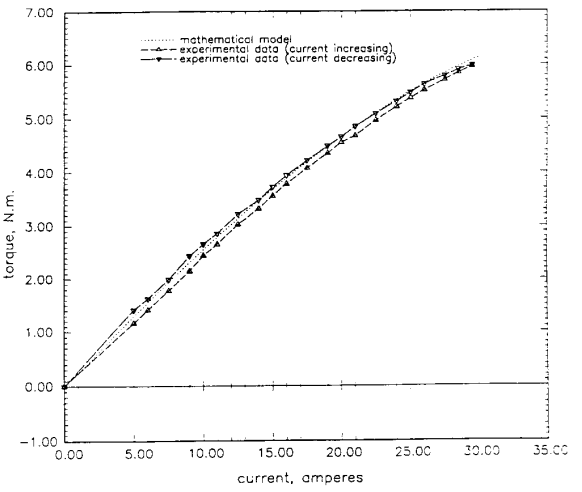

Figure 13: Experimental and modelled torque values, θ=83.0 degrees.

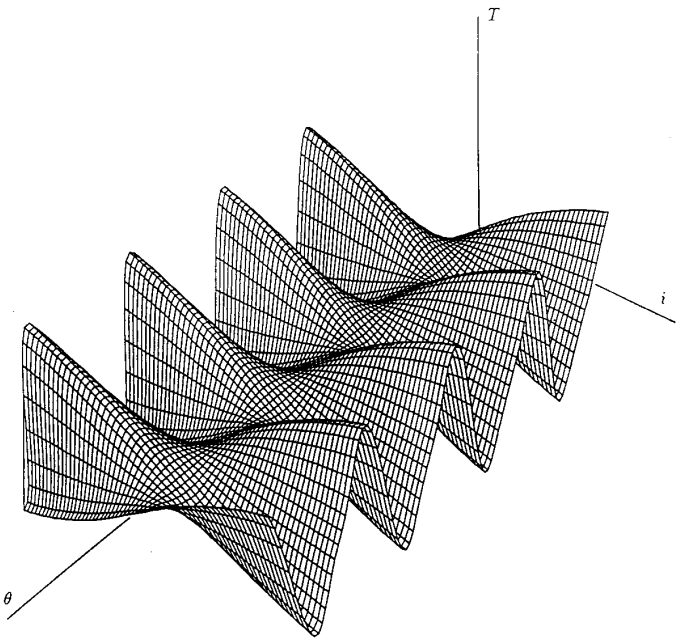

Figure 14: Torque surface for a line-to-line phase winding corresponding to the mathematical model.

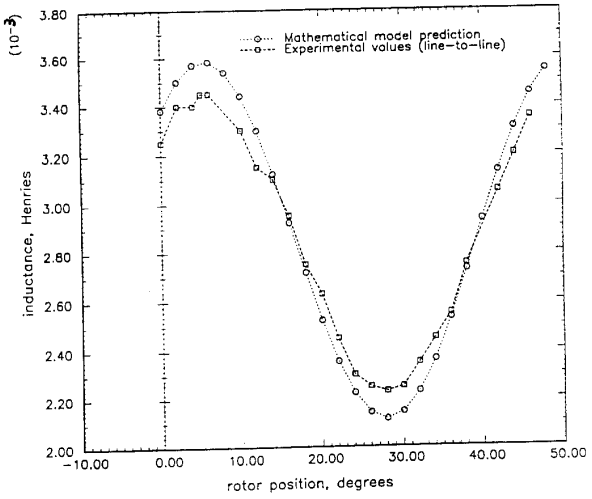

Figure 15: Experimental and predicted values of phase winding inductance (line-to-line).

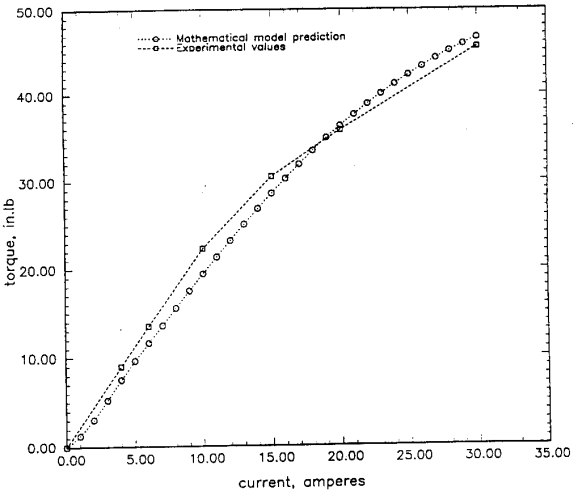

Figure 16: Experimental and predicted plots of torque vs. current, ω = 200 rpm.